Dual-Band Infrared Detectors Made on High-Quality HgCdTe Epilayers Grown by Molecular Beam Epitaxy on CdZnTe or CdTe/Ge Substrates

P. BALLET,[1] F. NOËL,[1] F. POTTIER,[1] S. PLISSARD,[1] J.P. ZANATTA,[1] J. BAYLET,[1] O. GRAVRAND,[1] E. DE BORNIOL,[1] S. MARTIN,[1] P. CASTELEIN,[1] J.P. CHAMONAL,[1] A. MILLION,[1] and G. DESTEFANIS[1,2]

1.—CEA-DRT-LETI/DOPT/Laboratoire Infra-Rouge, CEA Grenoble, 38054 Grenoble, France. 2.—E-mail: gerard.destefanis@cea.fr

In this paper, we present all the successive steps for realizing dual-band infrared detectors operating in the mid-wavelength infrared (MWIR) band. High crystalline quality HgCdTe multilayer stacks have been grown by molecular beam epitaxy (MBE) on CdZnTe and CdTe/Ge substrates. Material characterization in the light of high-resolution x-ray diffraction (HRXRD) results and dislocation density measurements are exposed in detail. These characterizations show some striking differences between structures grown on the two kinds of substrates. Device processing and readout circuit for 128×128 focal-plane array (FPA) fabrication are described. The electro-optical characteristics of the devices show that devices grown on Ge match those grown on CdZnTe substrates in terms of responsivity, noise measurements, and operability.

Key words: HgCdTe, molecular beam epitaxy (MBE), CdTe/Ge substrates, CdZnTe substrates

INTRODUCTION

There is an increasing interest in the development of multispectral infrared photodetectors.[1,2] In principle, the detection in two different bands or at two different wavelengths within the same band allows for the absolute determination of the temperature of the scene providing a constant emissivity over the spectral range. Mercury cadmium telluride (MCT) is the material of choice for this kind of application, as it enables a wide range of wavelengths to be detected by simply adjusting the cadmium fraction. Molecular beam epitaxy (MBE) is then particularly suited for growing multiple band structures, as it allows for stacking several absorbing layers of different cadmium composition.

In this paper, we focus on the MBE growth and complete realization of dual-band focal plane arrays (FPAs) detecting in the mid-wavelength infrared (MWIR) band. We present results obtained for structures grown on conventional (211)B CdZnTe

substrates but also on CdTe/Ge substrates. This latter type of substrate gets extremely attractive when considering the much larger area available compared to CdZnTe substrates.

The paper is divided in sections dealing with epitaxial growth and material characterization, device processing, readout circuit and flip-chip hybridization, and electro-optic characteristics.

EPITAXIAL GROWTH

Dual-band detectors consist of a multilayer stack grown by MBE on a (211)B CdZnTe substrate with a zinc nominal fraction of 4% or CdTe/Ge substrate. Growth is carried out in a mercury-dedicated Riber (Paris, France) 32P system. Details about the CdTe/Ge growth can be found in Refs. 3 and 4. The structure of the multilayer does not depend on the substrate nature. The growth temperature is about 180°C for MCT. It is adjusted for each layer to account for the mercury fraction of the layers. Careful adjustment of these temperatures together with accurate monitoring of the cadmium and tellurium fluxes is essential to prevent any

668

Ballet, Noël, Pottier, Plissard, Zanatta, Baylet, Gravrand, de Borniol, Martin, Castelein, Chamonal, Million, and Destefanis

degradation of the material quality throughout the structure.

A typical, secondary ion-mass spectrometry (SIMS) profile for cadmium and mercury is displayed in Fig. 1. The cadmium and mercury signals have been normalized to the Te signal that is unity for the whole stack. The structure consists of a thick layer with cadmium fraction of 0.4, allowing for the detection at the shortest wavelength (MWIR1), followed by a barrier and the second detection layer with 0.3 cadmium fraction (MWIR2). The stack is terminated by a surface bandgap widening layer. The first few microns of the first layer are indium doped in the 10^{17} cm^{-3} range to provide a common n contact for the diode array. The growth rate is kept constant for all layers, and the cadmium composition variation throughout the structure is obtained by continuously varying the cadmium flux so that no growth interrupts have to be implemented.

MATERIAL CHARACTERIZATION

Surface inspection, high resolution x-ray diffraction (HRXRD) mapping, and Fourier transform infrared (FTIR) optical transmission are routinely performed to get access to the crystalline and compositional characteristics of the epitaxial structures. Surfaces are smooth and mirrorlike. The surface microscopic-defect density is in the mid-10^{2} cm^{-2} range. This density is statistically found to be slightly larger compared to a single-layer growth. This is because the multilayer nature of the structure makes the substrate temperature adjustment more difficult. Full-width at half-maximum (FWHM) of the HRXRD peaks of structures grown on CdZnTe and CdTe/Ge are displayed in Figs. 2 and 3, respectively. Figure 2 also shows the map of the initial CdZnTe substrate for comparison. To clearly show the difference between a structure grown on CdZnTe and CdTe/Ge substrates, we have chosen to display a CdZnTe substrate that is very inhomogeneous, as can be seen on the map of Fig. 2. This is to
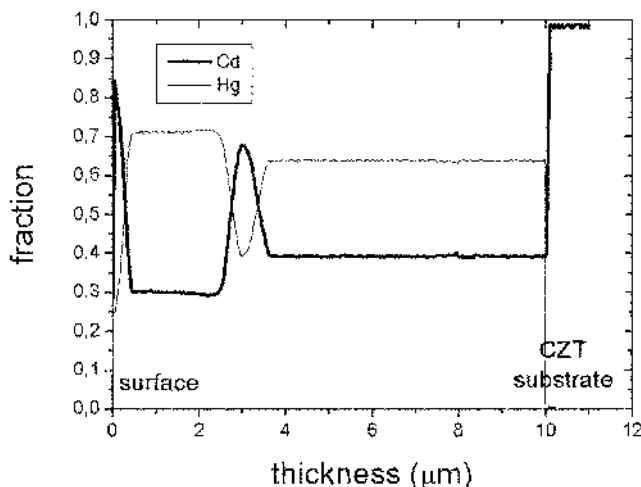
show that any inhomogeneity is reproduced by the epitaxial layer. On the other hand, structures grown on CdTe/Ge are homogeneous in nature; the standard deviation is 12 arcsec only, which is 10% of the mean FWHM value, while it is 25% in the case of Fig. 2. For structures grown on CdTe/Ge, any deviation from the mean value is due to nonuniformity in substrate heating or compositional dispersion only. It has to be noted that absolute FWHM values are always larger for CdTe/Ge-based structures and that the degradation of this value with respect to that of the substrate stays in the 10–40 arcsec range for both types of structures. This degradation is usually larger than that observed for a monolayer structure, again, because of the increased difficulty in maintaining the ideal growth temperature for each layer.
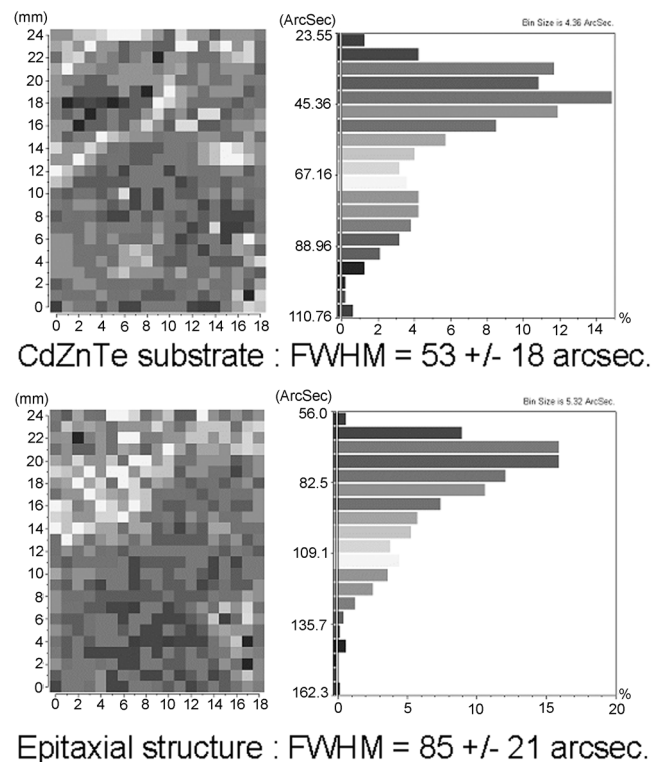
CdZnTe substrate : FWHM = 53 +/- 18 arcsec.

Epitaxial structure : FWHM = 85 +/- 21 arcsec.

Fig. 2. Mapping of the FWHM of the CdZnTe substrate (top) and subsequent epitaxial structure (bottom) together with histograms of FWHM values.

Fig. 1. The Cd and Hg SIMS profile of a two-color multilayer structure grown on a CdZnTe substrate.
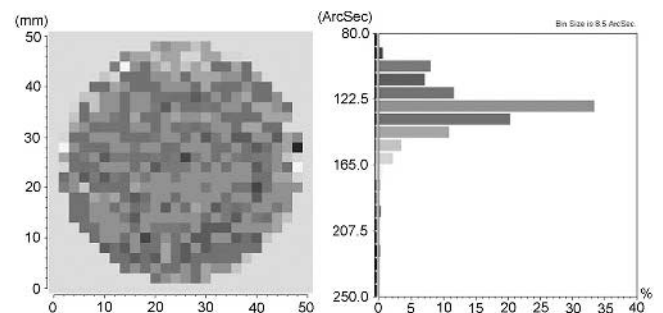
Fig. 3. Mapping of the FWHM of an epitaxial structure grown on the CdTe/Ge substrate together with histograms of FWHM values. The mean FWHM is 128 arcsec, and the standard deviation is 12 arcsec.

We have measured dislocation densities after appropriate etching of the surface. They are in the high mid-10^5 cm^{-2} and 10^7 cm^{-2} for structures grown on CdZnTe and CdTe/Ge, respectively. Again, the densities measured on stacked structures grown on CdZnTe substrates are about twice those measured on single-layer structures. This can be understood in terms of variation of the crystal lattice parameter along the growth axis because of composition variations.

Cutoff wavelengths together with structure total thickness are determined post-epitaxy through a fitting procedure to a FTIR spectrum. This procedure involves a simulation software taking into account all reflection and transmission at each interface. Input data are the real and imaginary part of the optical index for each layer. The absorption properties have been deduced from literature data,[5–7] while the real part of the refraction indexes have been experimentally derived from single-layer FTIR data, assuming that the change in periodicity in the interference oscillations when approaching the bandgap is only due to changes in index of refraction. We found the cutoff wavelengths estimated after epitaxy to be systematically lower than those measured electro-optically on the device at 77 K. However, this shift never exceeds 0.3 µm at 77 K and is roughly independent of the wavelength range. A similar issue has been pointed out in a recent paper by Moazzami et al.[8] and is attributed by the authors to a lack of knowledge of the absorption properties of HgCdTe especially at low temperature.

DEVICE PROCESSING AND READOUT CIRCUIT

The cross section of a multispectral device is presented in Fig. 4. It consists of two back-to-back n-on-p photodiodes. The MWIR1 diode is realized during epitaxy by simply doping part of the first absorbing layer. The MWIR2 junction is obtained using an implantation process according to the fabrication of a standard, single wavelength diode.

Mesas have been separated using dry or wet etching. A scanning electron micrograph is shown in Fig. 5. The pixel pitch is 50 µm, and typical filling factors are about 60%. Dry etching allows for larger fill factors and smaller pixel pitch. It is discussed in detail in another paper.[9] All the results presented in this paper are for a pitch of 50 µm.
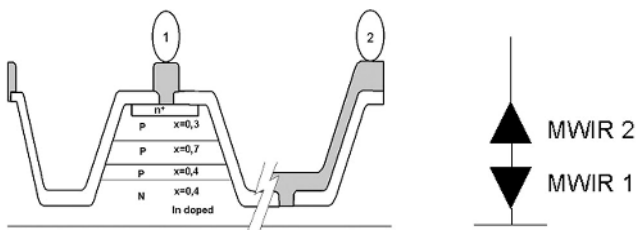

Fig. 4. The dual-band detector architecture with a single indium bump per pixel.

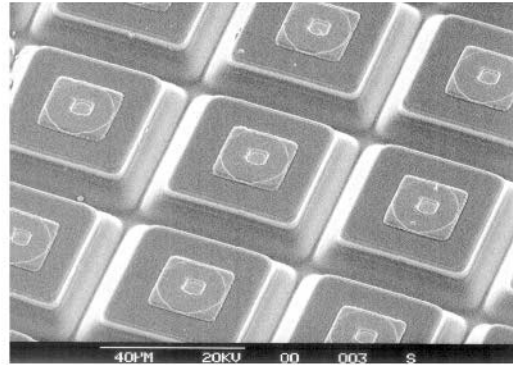Fig. 5. The SEM image of a dual-band detector array with a 50-µm pixel pitch.

The p-type doping levels are adjusted by controlling the Hg vacancy concentration by means of thermal annealing. This process has to be adjusted for two-color detectors because of the presence of the indium doping that should not be deactivated nor compensated by too strong anneals.

The other steps of the process are equivalent to those of the LETI-LIR (Grenoble, France) planar technology. Details may be found in Ref. 10.

The detector is hybridized to the complementary metal-oxide semiconductor (CMOS) circuit using the flip-chip technology. The CMOS circuit scheme is displayed in Fig. 6. It has a 128 × 128 complexity and allows for the sequential reading of the two back-to-back diodes. Each diode being read through the direct polarization of the other. The device is thus spatially coherent but presents a temporal shift because of sequential addressing of the two bands. The main advantage of this circuit is that it allows for an independent optimization of the two channels. The capacitance, integration times, and readout buffers have been independently calibrated to account for the differences in current between the two diodes.
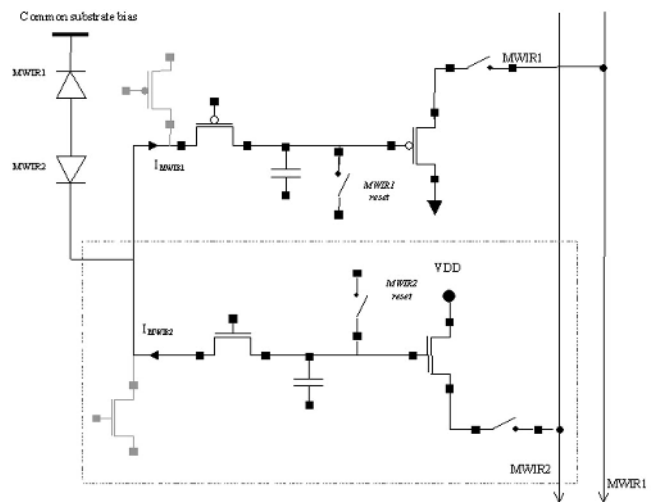

Fig. 6. Circuit layout. The MWIR1 and MWIR2 back-to-back diodes are read sequentially. The two channels have been independently optimized in terms of capacitance and integration times.

670

Ballet, Noël, Pottier, Plissard, Zanatta, Baylet, Gravrand, de Borniol,
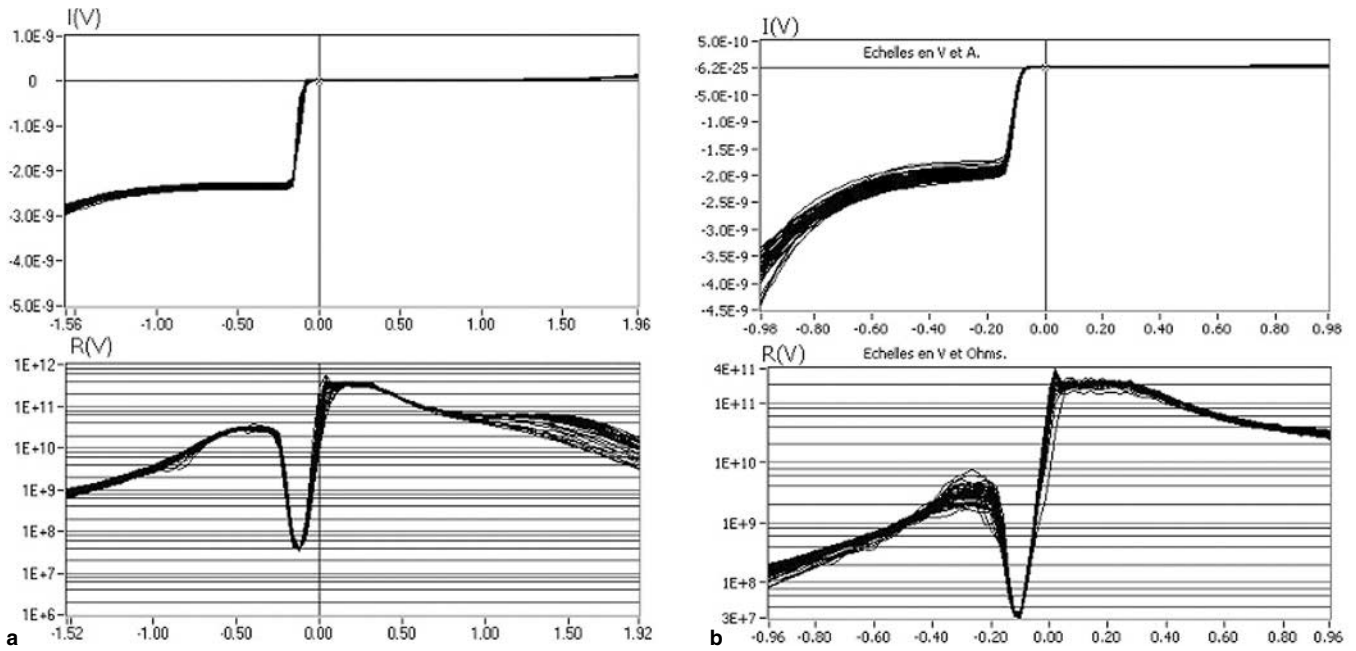Martin, Castelein, Chamonal, Million, and Destefanis

Fig. 7. The I-V and R-V curves for devices grown on (a) CdZnTe and (b) Ge. The scales are volts, amps, and ohms. The negative voltage corresponds to the reverse of the MWIR2 diode, while the positive voltage corresponds to the reverse of the MWIR1 diode.

ELECTRO-OPTICAL CHARACTERIZATION

The electrical characteristics of devices grown on CdZnTe or Ge substrates are equivalent with breakdown voltages and maximum impedance close to or equal to those usually measured on conventional, planar single-band diodes. Figure 7 displays I-V and resistance-voltage (R-V) curves for devices grown on CdZnTe and Ge substrates. The characteristics are well packed with no significant dispersion. The difference in the impedance of the MWIR2 diode between the two devices can be related to the difference in cutoff wavelength.

A typical spectral response for the two diodes is plotted in Fig. 8. The MWIR1 and MWIR2 diodes have good spectral signature with cutoff wavelength equal to 3.3 μm and 5.4 μm, respectively.
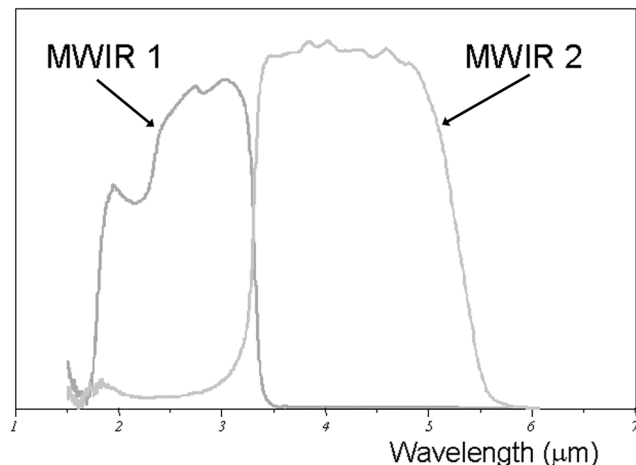

Fig. 8. Typical, normalized 77-K spectral response. The MWIR1 diode cuts at about 3.3 μm, while MWIR2 has a cutoff wavelength of 5.4 μm.

More complete electro-optical characterization is available through Figs. 9 and 10, where the responsivity and the noise-equivalent temperature difference (NETD) together with the associated operabilities are plotted for nine devices including three that have been grown on CdTe/Ge substrates. Operability is here defined by the plus or minus three times the standard deviation interval. The measurements have been carried out with a focal-plane temperature of 77 K and a scene temperature of 298 K. The field of view is 30°. The MWIR1 and MWIR2 integration times are 4 ms and 1.5 ms, respectively.

From Fig. 8, it can be seen that the operability in responsivity is higher than 99% in the two bands and that the values obtained for devices grown on Ge match those for devices grown on conventional CdZnTe substrates. Most of the time, the dispersion observed is smaller for devices grown on CdTe/Ge substrates. Data about NETD show again that the devices grown on Ge compare fairly well with the others. The operability in the MWIR2 band is the highest for these devices. All devices are background limited in the MWIR1 band, while most of them are very close to background limited infrared photodetector (BLIP) in the MWIR2 band with defect density less than 3%. The deviation from the background-limited regime has to be related to the mesa technology because conventional planar diodes are always BLIP for the wavelength considered here. In any case, it is clear that the deviation does not depend of the choice of the substrate nature.

Finally, Fig. 11 displays a double image taken from a Ge-grown FPA (device 2566). The bottom image is for the shortest wavelength (cutoff wavelength:

Dual-Band Infrared Detectors Made on High-Quality HgCdTe Epilayers
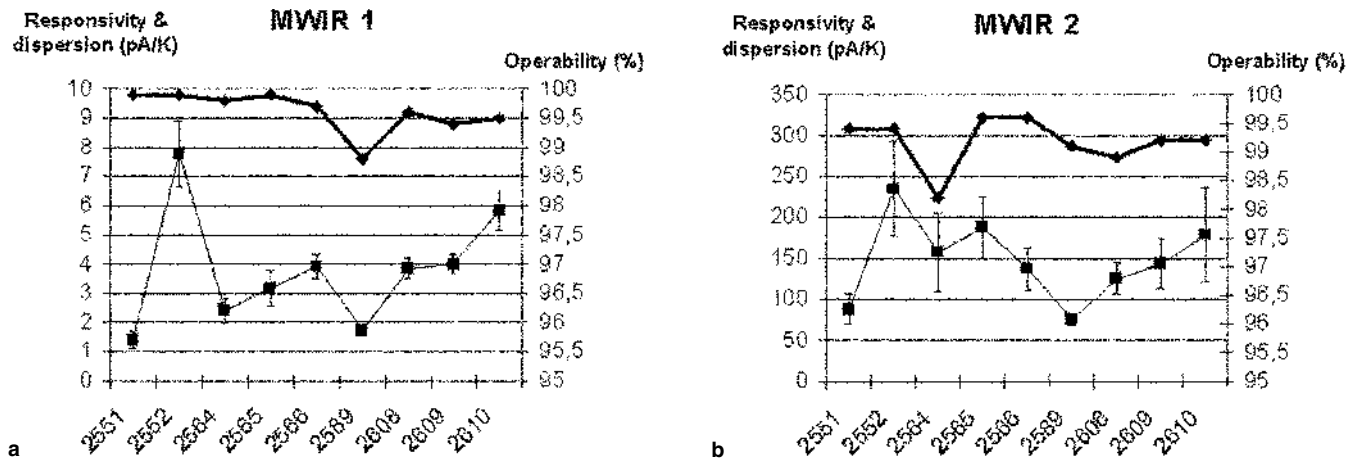Grown by Molecular Beam Epitaxy on CdZnTe or CdTe/Ge Substrates

671

Fig. 9. Plots of the responsivity (square) and associated dispersion (error bars) for the (a) MWIR1 and (b) MWIR2 diodes in several dual-band detector devices. The operability defined in the plus or minus three times the standard deviation interval is plotted with diamond for each band. Devices 2566, 2608, and 2609 have been grown on Ge substrates.
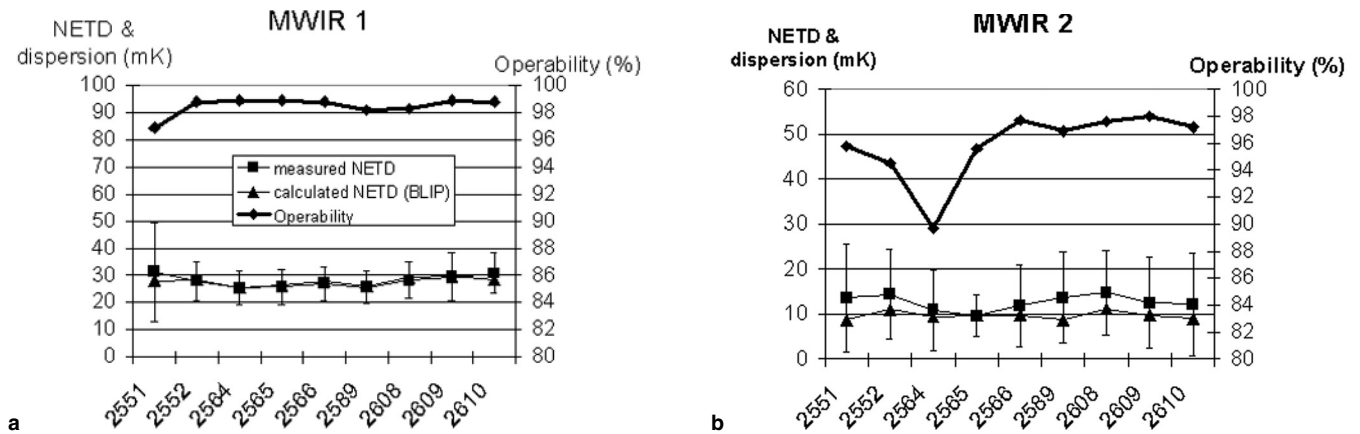

Fig. 10. Plots of the NETD (square) and associated dispersion (error bars) for the (a) MWIR1 and (b) MWIR2 diodes in several dual-band detector devices. The operability defined in the plus or minus three times the standard deviation interval is plotted with diamond for each band. The background-limited regime is also plotted for comparison (triangles). Devices 2566, 2608, and 2609 have been grown on Ge substrates.

Fig. 11. Example of a dual-band image showing a car in a parking lot with back lights on. (a) longest wavelength image (MWIR2) and (b) short wavelength (MWIR1) image. The device used is grown on CdTe/Ge (2566).

672

Ballet, Noël, Pottier, Plissard, Zanatta, Baylet, Gravrand, de Borniol,
Martin, Castelein, Chamonal, Million, and Destefanis

3.5 μm). Note that the backlights of the car can only be seen in the bottom image. Open circuit defects have been software corrected.

SUMMARY

We have shown in this paper that high-quality HgCdTe multilayers have been grown on CdZnTe and CdTe/Ge substrates. All the devices made out of these two kinds of structures show equivalent and very good electro-optical characteristics. However, most of them exhibit a small deviation in the BLIP value for the MWIR2 diode. This point is currently under investigation in our laboratory. This paper clearly shows that the devices grown on CdTe/Ge really match those grown on CdZnTe substrates despite some important differences in material properties, namely, wider diffraction peaks and much larger dislocation densities. This opens the way toward large-area epitaxy and shows the potential of this technology for future industrialization.

REFERENCES

1. W.E. Tennant et al., *J. Electron. Mater.* 30, 590 (2001).
2. J. Baylet, J.P. Zanatta, D. Chance, O. Gravrand, F. Rothan, E. De Borniol, P. Castelein, J.P. Chamonal, M. Ravetto, and G. Destefanis, *Proc. SPIE* 4721, 134 (2002).
3. J.P. Zanatta, P. Ferret, P. Duvaut, S. Isselin, G. Theret, G. Rolland, and A. Million, *J. Cryst. Growth* 184/185, 1297 (1998).
4. J.P. Zanatta, P. Ferret, G. Theret, A. Million, M. Wolny, M. Chamonal, and G. Destefanis, *J. Electron. Mater.* 27, 542 (1998).
5. J.L. Pautrat and N. Magnea, EMIS datareviews Series no. 10 (INSPEC, IEE, 1994), p. 76.
6. E. Finkman and S.E. Schacham, *J. Appl. Phys.* 56, 2896 (1984).
7. K.H. Hermann, M. Happ, H. Kissel, K.P. Mollmann, J.W. Tomm, C.R. Becker, M.M. Kraus, S. Yuang, and G. Landwehr, *J. Appl. Phys.* 73, 3486 (1993).
8. K. Moazzami, D. Liao, J.D. Phillips, D.L. Lee, M. Carmody, M. Zandian, and D.D. Edwall, *J. Electron. Mater.* 32, 646 (2003).
9. J. Baylet et al., in this issue.
10. G.L. Destéfanis, *Semicond. Sci. Technol.* 6, C88 (1991).